JOURNAL OF APPLIED ELECTROCHEMISTRY 23 (1993) 531–546

REVIEWS OF APPLIED ELECTROCHEMISTRY 36

Some *in situ* STM contributions to the characterization of electrochemical systems*

A. GONZÁLEZ-MARTÍN, R. C. BHARDWAJ, J. O'M. BOCKRIS

Surface Electrochemistry Laboratory, Department of Chemistry, Texas A&M University, College Station, TX 77843, USA

Received 21 July 1992; revised 30 September 1992

We present a critical review on the use of STM as an *in situ* technique to characterize electrochemical systems based on the work performed in our laboratory. Contributions of *in situ* STM studies include: (i) atomic resolution of electrodeposited lead on graphite; (ii) imaging of modifications on metallic electrode surfaces induced by electrochemical oxidation-reduction processes; (iii) imaging of corrosion process on aluminium and Al–Ta alloy electrodes in NaCl solution; (iv) characterization of semiconductor-solution interfaces. These studies allowed: (a) establishment of STM as a technique which, for some systems, yields atomic resolution of metallic surfaces in air and in solution; (b) establishment of a mechanism for the electrochemical growth of oxide films on metal electrodes; (c) establishment of a corresponding mechanism for the reduction of those electrochemically grown oxide films; (d) direct monitoring of corrosion processes on a scale of nm to μm; and (e) determination of the presence of surface states and their energy position at the semiconductor–solution interfaces.

1. Introduction

It is well recognized that electrode properties depend on the structure of the electrode surface. To identify this relationship requires an *in situ* technique capable of imaging the surface at high resolution (atomic to micrometer resolution). Few techniques are able to provide information on surfaces at high resolution (i.e. LEED, XPS, SEM, and Auger). However, such techniques are not directly applicable to electrodes because of the presence of solution; they require vacuum conditions.

Scanning tunnelling microscope (STM) techniques can provide real space imaging of structural, electronic, and chemical surface properties at high resolution [1, 2]. The use of *in situ* STM in an electrolytic environment was first demonstrated by Sonnenfeld and Hansma [3]. Since then STM has been applied to many fields in electrochemistry: electrodeposition of metals [e.g. 4–6]; adsorption of atoms and molecules on electrodes [e.g. 7]; oxidation–reduction of electrode surfaces [e.g. 8–13]; corrosion [e.g. 14, 15]; and semiconductors [e.g. 16–19]. In this paper we present a review of STM researches on various areas of electrochemistry carried out at Texas A&M University since 1988, showing the capability of this technique to provide information on processes occurring at the surface of electrodes unrivalled by any other technique.

2. Experimental details

A NanoScope I (Digital Instrument Inc., California) was used in all the experiments discussed here. This instrument operates only in the constant current mode. Details on the experimental setup are given elsewhere [5].

STM tips for the studies in solution were purchased from two companies: FHC, Brunswick and Longreach Scientific Company. They were made of tungsten and covered with an epoxy layer up to the operational tip to decrease the faradaic current. For the work on lead electrodeposited on graphite [5] and platinum reduction–oxidation in 0.01 M $NaClO_4$ [11], tips were made of platinum and covered with a glass layer up to the operational tip.

The electrochemical potentials of the electrode and tip were independently controlled by the use of a four-electrode potentiostat [16] constructed in this laboratory†. A saturated calomel electrode (SCE) was used as the reference electrode, and a platinum wire (99.99%) was the counter electrode. The electrochemical potential of the tip was held in the double layer region, where the faradaic current is minimal. Typical values for the faradaic current were below 0.1 nA.

During *in situ* measurements, the position of the tip was not mechanically moved, unless otherwise indicated.

The tunnelling current is indicated in each Figure. Chemicals were of reagent grade quality and used

† For the work on Pb electrodeposition on graphite [5] and Pt reduction–oxidation in 0.01 M $NaClO_4$ [11], the potential of the working electrode was adjusted by using a battery power voltage source.

* This paper is dedicated to Professor Brian E. Conway on the occasion of his 65th birthday and in recognition of his outstanding contribution to electrochemistry.

0021-891X

without further purification. Solutions were prepared with Millipore water (resistance about 18 MΩ cm).

3. Results and discussion

3.1. *Electrodeposition:* in situ *studies of lead electrodeposited on graphite substrate*

The field of electrocrystallization started in 1834 when Faraday's laws were enunciated. Thus, the study of electrocrystallization is one of the oldest parts of electrochemistry. However, *in situ* information at atomic levels on the mechanism of the reaction, and the structure and ageing of the deposits could not be obtained until the use of STM in recent years.

The first *in situ* study showing an electrodeposited metal at atomic levels was carried out by Szklarczyk *et al.* [5, 20]. Here, lead was electrodeposited on highly oriented pyrolitic graphite (HOPG). This work not only established STM as a powerful technique for fundamental studies in electrodeposition but also addressed the question of the capability of STM to show atomic resolution of metallic surfaces. Very few publications showing atomic resolution of metal surfaces were published previously to this study, and none in electrolytic solution: aluminium in vacuum [21] and gold in air and in vacuum [22]. In the case of platinum, atomic resolution was achieved only after chemisorption of molecules, such as iodine [23], NO and CO [24].

Figure 1 shows STM images at atomic levels of the HOPG electrode surface in air (Fig. 1a) and in solution (0.01 M $NaClO_4$) under potential control (Fig. 1b). The distance between two adjacent equivalent carbon atoms is 0.23 ± 0.02 nm in air and 0.23 ± 0.03 nm in solution (Table 1), whereas for two non-equivalent carbon atoms (benzene ring) the distance is 0.14 ± 0.02 nm. The corrugation was 0.08–0.15 nm. These values are in agreement with those reported in the literature [3].

Figure 2 shows the atomic resolution obtained by *in situ* STM of lead electrodeposited on HOPG. The lead film was obtained by depositing a thick layer of lead and then electropolishing the surface of the deposit by electrochemical dissolution. The final thickness of the layer was about 80 monolayers. The STM image for this electrode was taken at −0.2 V vs SCE. Figure 3 shows the STM image for lead deposit in air, after removing the solution and washing the surface of the electrode with water. The interatomic distance between two adjacent lead atoms for the image obtained in solution is 0.36 ± 0.03 nm, whereas in air is 0.31 ± 0.04 nm (Table 1). The Pb–Pb distances cited in the literature vary from 0.30 [25] to 0.35 nm [26], 0.36 nm [27] and 0.39 nm [28].

Figures 2 and 3 also allow the determination of the crystallographic plane of the film. In Fig. 2, an angle of 90 ± 5° and distances of 0.36 nm are detected, which corresponds to the [1 0 0] plane. This is in agreement with the view that the preferred orientation axes for lead electrodeposits is [1 0 0], [29]. However, most

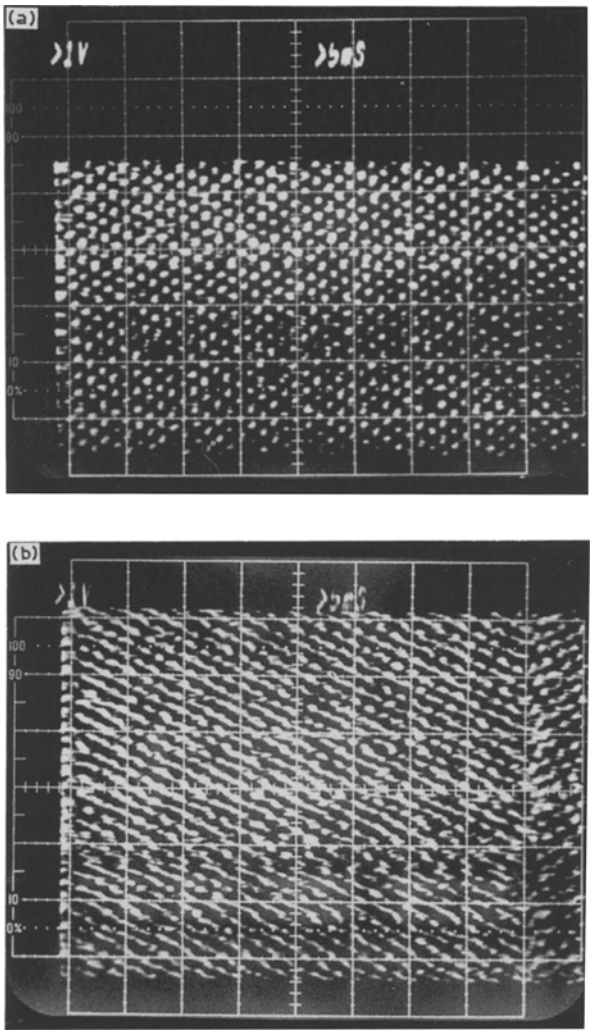

Fig. 1. STM images of HOPG surface detected in (a) air and (b) solution. $XY = 0.9 \times 0.9\,(\mathrm{nm})^2$; $V_{bias} = -30$ mV; $i_{tun} = 1.5$ nA.

electrodeposited films are polycrystalline [30], where the ratio between different faces depends on the condition of electrodeposition, because the rate of growth of specific faces differs one from the other. Additionally, it seems that the application of the electropolishing procedure increases the degree of crystallographical uniformity on the surface. These reasons, together with the fact that the scanning area is small (7.2 nm × 7.2 nm), explains the fact that well-ordered lead lattice was observed instead of random-oriented lead atoms.

The fact that the images shown in Figs 2 and 3 represent a lead lattice, and not a graphite lattice, is supported by: (i) the amount of deposited lead was large enough fully to cover the HOPG substrate

Table 1. Interatomic distances determined by STM [5]

Figure	*Bond*	*Environment*	*Distance/nm*
1a	C–C	Air	0.24 ± 0.02
1b	C–C	10^{-2} M $NaClO_4$ + 10^{-3} M $Pb(ClO_4)_2$	0.24 ± 0.02
2	Pb–Pb	10^{-2} M $NaClO_4$ + 10^{-3} M $Pb(ClO_4)_2$	0.36 ± 0.03
3	Pb–Pb	Air	0.31 ± 0.04

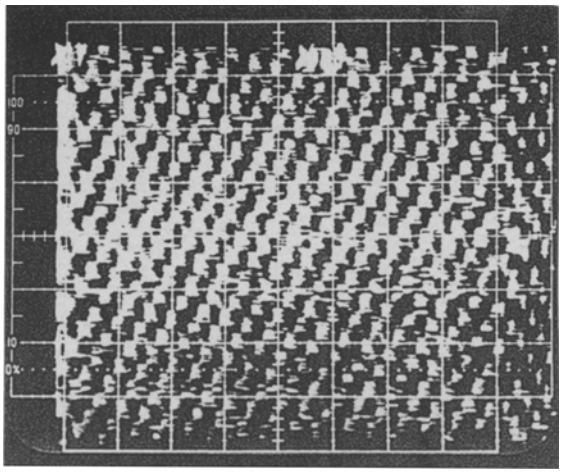

Fig. 2. STM images of lead deposited on HOPG surface detected in solution. $XY = 0.9 \times 0.9\,(\mathrm{nm})^2$; $V_{bias} = -30\,\mathrm{mV}$; $i_{tun} = 1.5\,\mathrm{nA}$.

(~ 30 nm thick); (ii) XPS studies of the electrode after the lead electrodeposition showed the presence of lead; (iii) the observed interatomic distances are greater than those for graphite (Table 1).

At this point the question about the possibility to observe atomic resolution for metals (in this case lead) should be addressed. The resolution of individual atoms by STM is related to local variations in the tunnelling current. These are commonly attributed to the presence of localized electronic states on the surface around the Fermi level, E_F, which contribute to the tunnelling current. In the bulk of the metal, the valence electrons are mostly delocalized. The situation on the surface may be different than in the bulk, because of the existence of localized electronic states. However, in general, the atomic corrugation on metal surfaces is expected to be much weaker than that of semiconductor surfaces for example. Now, the magnitude of how the location of electronic states is reflected on the atomic corrugation of the metal surface will depend on the outermost electronic shell, so it will be different for different metals. In addition, localized density of states can be induced by chemisorption, as in the case of platinum in air [22, 23] and solution [31, 32], rhodium in solution [33], and copper [34] and rhenium [35] in vacuum. In the case studied here, the location of electronic states on the lead surface induces a corrugation of about ~ 0.03 nm, which is sufficiently large to be detected by STM. This allows one to observe atomic resolution of the images. In more recent works, similar corrugations have been obtained for gold single crystals in solution [36, 37], and silver single crystal in vacuum [38].

Thus, this STM study of lead electrodeposited on HOPG showed: (i) that atomic resolution of lead in solution and in air was achieved for the first time, and (ii) that the deposit is crystalline, predominantly showing a [1 0 0] face. These findings can be directly applied to electrocatalysis, where the crystal face plays a determining role on the rate of reaction.

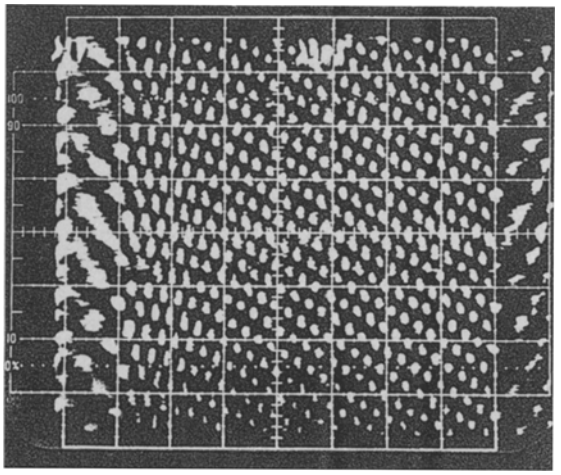

Fig. 3. STM images of lead deposited on HOPG surface detected in air. $XY = 0.9 \times 0.9\,(\mathrm{nm})^2$; $V_{bias} = -30\,\mathrm{mV}$; $i_{tun} = 1.5\,\mathrm{nA}$.

3.2. *Electrochemical oxidation–reduction of metals*

Before presenting *in situ* STM studies on electrochemical oxidation–reduction of metals, it is necessary to comment on the phenomenon of thermal drift. It has been recognized that thermal drift may be a problem inherent to the STM design [39]. This may be critical in studies where changes on the electrode surface are monitored as a function of time. In those cases, areas of about 1 μm^2 were studied [9, 10, 15]. This in turn reduced the effect of thermal drift, which was less than 0.24 nm min^{-1} when an area of 125 nm × 125 nm was scanned [15]. For this area, about 10 h are required to scan a completely different region considering a unidirectional thermal drift. However, thermal drift is a random process, which increases the time required to scan a completely different portion of the electrode. Therefore, changes observed on the surface as a function of time and/or potential correspond approximately to the same region, within the time that most of the *in situ* STM experiments were performed.

Another point that may be raised is the validity of the information given in the STM Figures as representative of the surface being examined. Each experiment was carried out at least twice, and similar results were observed (i.e. dependence of the modification of the surface with time and potential).

3.2.1. Polycrystalline platinum in 0.01 M $NaClO_4$. The surface structure of the electrode often changes during electrochemical reactions caused by the oxidation/reduction of the surface as well as by adsorption/desorption of metal atoms. This, in turn, has an effect on the reactivity of the electrode. *In situ* STM allows one to monitor these changes as a function of both the electrode potential and time at high resolution.

Several STM studies showing surface structure changes of noble metal electrodes due to potential cycles have been reported [12, 40–42]. Vazquez *et al.* [40] examined the platinum surface *ex situ* by STM after applying several potential cycles. Itaya *et al.* [12, 41, 42] showed the dependence of changes on the surface of the electrode with the number of cycles by *in situ* STM. However, STM images were recorded in the double layer region *after* the potential was cycled;

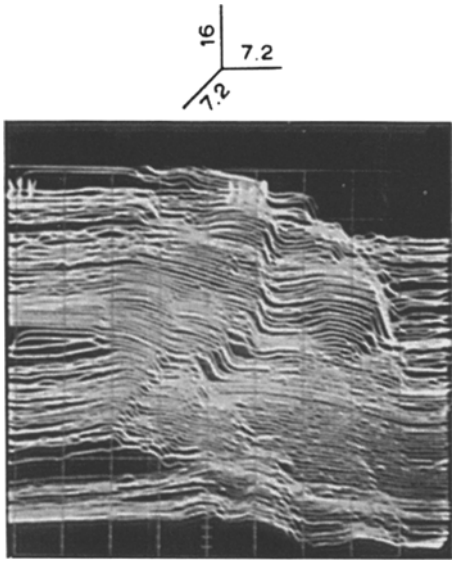

Fig. 4. STM image of platinum electrode registered in solution. E_{Pt} = 0.15 V vs NHE; i_{tun} = 15 nA.

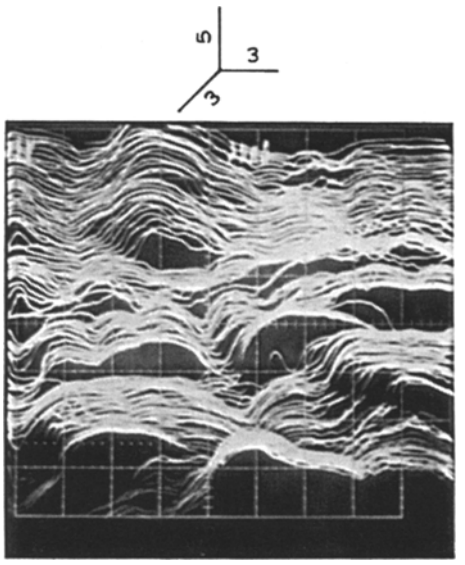

Fig. 6. STM image of platinum electrode registered in solution. E_{Pt} = 1.45 V vs NHE; i_{tun} = 10 nA.

no images were recorded, for example, during oxidation of the surface. Uosaki *et al.* [8] showed, *in situ*, real time monitoring of the surface structure changes by STM. In this work, the platinum surface was studied at reduction potentials *after* an oxidation pulse was applied. No images were recorded during electrochemical oxidation. The work of Szklarczyk *et al.* [11] is the only study showing changes of the surface of the platinum electrode during both oxidation and reduction processes by *in situ* STM. Part of those changes on the platinum surface are discussed here.

Figure 4 shows an *in situ* STM image of a platinum electrode immersed in a 10^{-2} M $NaClO_4$ solution. This image was recorded at 0.15 V vs NHE, that is the surface is free of an oxide film. A stepped surface is observed, with terraces of width of about 15–30 nm, and step heights of about 4–8 nm.

Figure 5 shows an *in situ* STM image of the same electrode during the application of a small oxidation potential (1.1 V vs NHE). Here, some changes on the structure of the surface were observed, i.e. the formation of small humps, of about 2–3 nm, in selective areas of the electrode (i.e. steps).

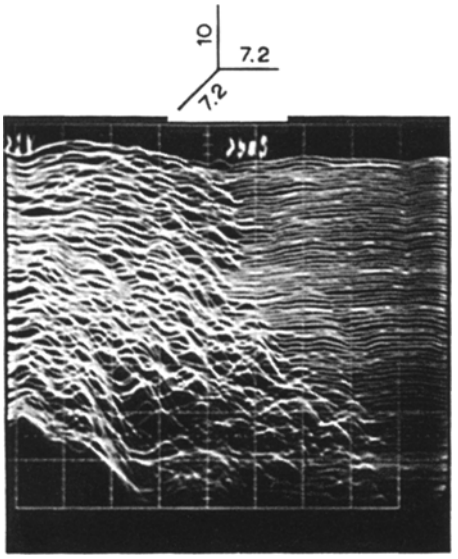

Fig. 5. STM image of platinum electrode registered in solution. E_{Pt} = 1.1 V vs NHE; i_{tun} = 15 nA.

Changing the potential in the negative direction to a sufficient extent caused the reduction of the oxide and produces the stepped surface shown in Fig. 4. A similar result was obtained by Uosaki *et al.* [8]: a stepped surface was obtained at the reduction potential after applying a small anodic potential. In addition, they observed reconstruction of the platinum surface with time, leading to the formation of the stepped surface.

Figure 6 shows the STM image registered at higher oxidation potentials (1.4 V vs NHE). The surface was no longer stepped but constructed of semispherical domains with flat tops, of dimensions about 6 nm. At this higher anodic potential the rate of oxidation was faster, leading to the formation of a more disordered oxide film. A stable image of the platinum surface at the reduction potential was obtained after 10 min. It is known by electrochemistry that the electrochemical reduction of that oxide is about 100 times faster than the time required to obtain a surface with no change as a function of time.† A mechanism for the reduction of the oxide film on platinum was then proposed: first, a fast electrochemical reduction of the oxide film; then, a slow crystallographic surface reconstruction, leading to a minimization of the surface energy.

3.2.2. In situ *studies of polycrystalline aluminium in 0.01 M NaOH.* Another important branch of electrochemistry is the study of non-noble metals, where the stability of these materials is affected by corrosion processes. The study of the corrosion effect on the structure of the surface of those metals has been

† Similar long time surface reconstruction has been observed for gold electrodes [43].

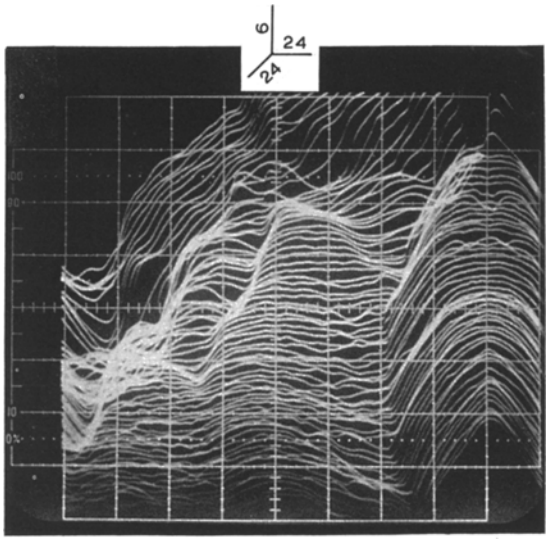

Fig. 7. STM image of aluminium electrode in air. $V_{bias} = -1.06$ V; $i_{tun} = 1.0$ nA.

attempted in the past (i.e. Fe [43], Al [45, 46]). However, the approach taken to study the changes in the surface has been rather indirect: samples were analysed using either electrochemical techniques to determine the pitting potential, or *ex situ* techniques such as SEM to define the corrosion behaviour after the corrosion process was induced by electrochemical means.

In the past, few papers have been published using *in situ* STM to study corrosion-related processes: stainless steel in aqueous chloride media at a resolution of 10 nm [14, 47], and dissolution of nickel in diluted sulphuric acid under potentiostatic controlled conditions [48].

Here, we present the work done in the study of the effect of reduction–oxidation processes in aluminium in NaOH solution [9] and iron in borate buffer [10], using *in situ* STM. A study of the corrosion on polycrystalline aluminium and Al–Ta alloy in NaCl solution [15] is also presented in Section 3.3.

Figure 7 shows an STM image of an aluminium electrode in air. The image looks rather rough, with dome-like structures with heights of 2–5 nm and steps of 10–12 nm. The initial surface is covered with a native oxide film [49].

Figure 8 shows an STM image of the same electrode in solution (NaOH 0.01 M), where the electrochemical potential of the aluminium sample was held at a reduction potential (-1.135 V vs NHE). Just after applying this reduction potential, the surface looks still rough (Fig. 8a) (i.e. well defined steps of 5–10 nm). Nevertheless, surface features are better revealed than for the image in air. Similar 'improvement' of the resolution of the STM images after immersion in solution was observed by Bard *et al.* [14] for stainless steel immersed in NaCl solution. This 'improvement' of the STM images once the electrode is immersed in solution, is due to dissolution of the insulating surface layer. In the case of aluminium immersed in alkali solutions, the surface remains active and dissolves at

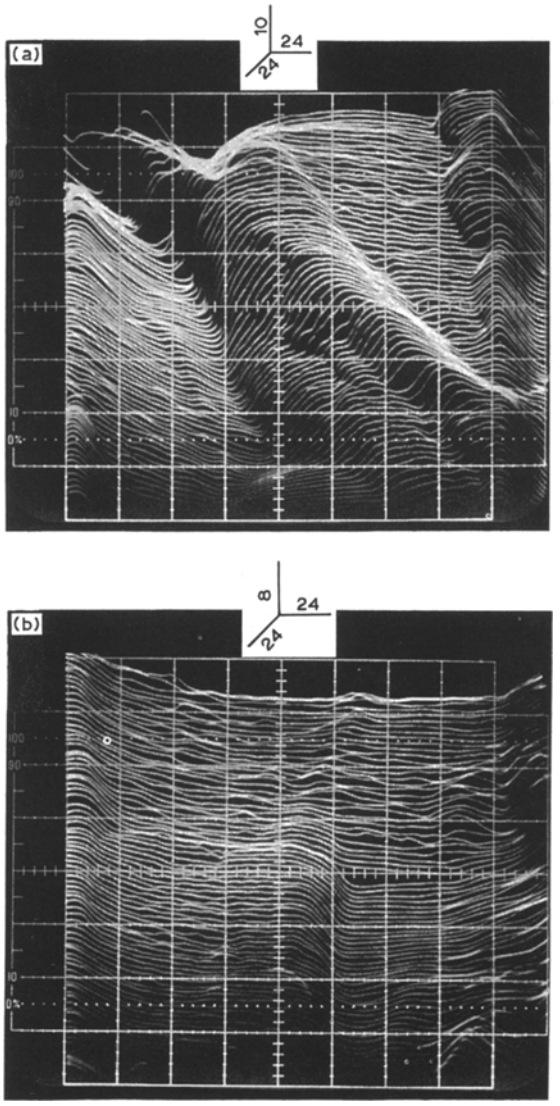

Fig. 8. STM image of aluminium electrode in solution at $V_{Al} = -1.135$ V; $V_W = -0.265$ V vs NHE; $i_{tun} = 1.0$ nA. (a) immediately after immersion; (b) after 5 min.

potential more negative than -1.0 V vs NHE, being free of an oxide film [50, 51].

Figure 8(b) shows an STM image of the electrode taken 5 min after immersion in the solution and application of a reduction potential. Here, the surface looks smoother than before: steps of 2–4 nm and terraces 2–4 times longer. Similar results were obtained by Uosaki *et al.* [8] for the reduction of an oxide film electrochemically formed on a platinum electrode by application of a small anodic potential: at longer times of reduction, smoother terraces steps of mono to several atomic heights were formed.

Figure 9 shows the STM image of the aluminium electrode 2 min after applying an anodic potential (-1.05 V vs NHE). The formation of small humps (~ 1 nm), like nucleation centres, were observed in selective regions of the surface, i.e. steps. A similar result was observed for the work done on Pt/$NaClO_4$ [11]: formation of small humps in selective parts of the surface.

An image as shown in Fig. 8(b) was obtained 5 min after the electrochemical potential of the sample was

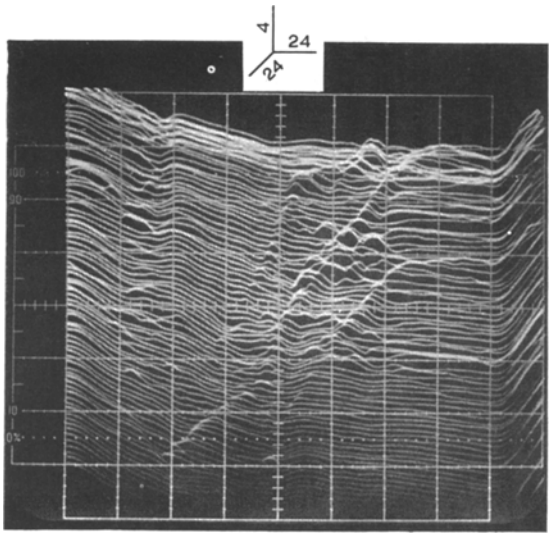

Fig. 9. STM image of aluminium electrode in solution after 2 min at $V_{Al} = -1.05$ V; $V_W = -0.185$ V vs NHE; $i_{tun} = 1.0$ nA.

brought back to the reduction potential (1.135 V vs NHE). The stepped surface appears again, and the small humps previously formed disappeared. Thus, the oxide film grown at −1.05 V vs NHE was removed within that time. Again, a similar result was obtained in the work of $Pt/NaClO_4$ [11], where the initial stepped surface was produced after the reduction of the oxide film formed at small anodic potentials.

Application of higher anodic potentials (−0.975 V vs NHE) produced a rougher surface, as shown in Fig. 10. The big humps and noisy terraces represent the growth of a non-uniform oxide. A smooth surface was observed at the reduction potential only after 20 min.

3.2.3. Polycrystalline iron in borate buffer. Figure 11(a) shows the STM image obtained 3 min after the sample was immersed in the borate buffer solution, where the electrochemical potential of iron was held at a reduction value (−0.75 V vs NHE). Figures 11(b) and (c)

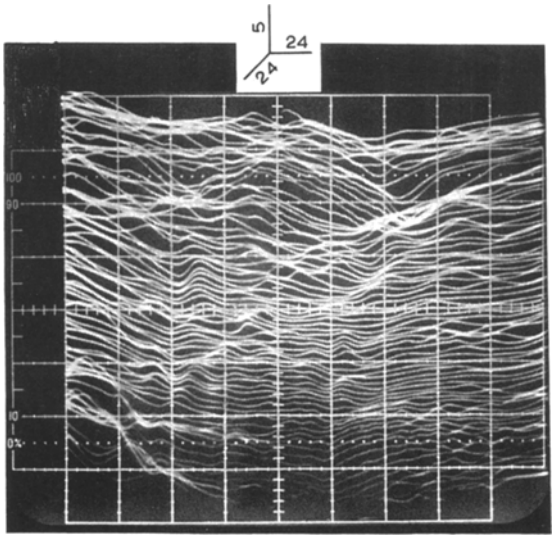

Fig. 10. STM image of aluminium electrode in solution after 2 min at $V_{Al} = -0.975$ V; $V_W = -0.185$ V vs NHE; $i_{tun} = 1.0$ nA.

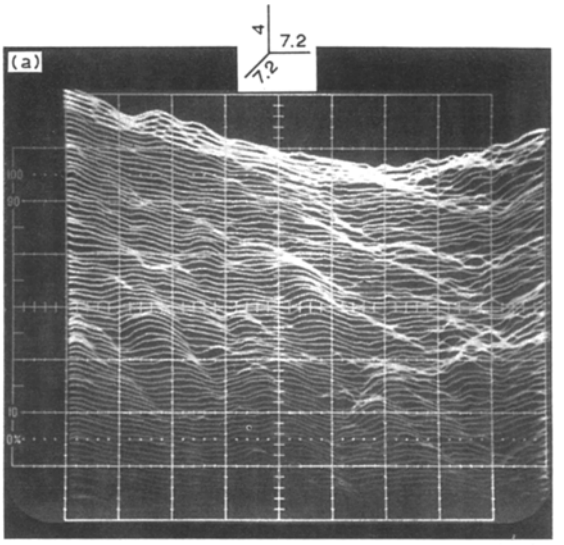

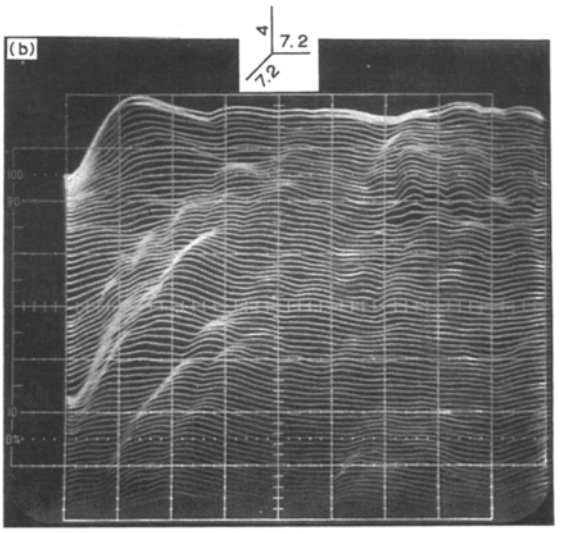

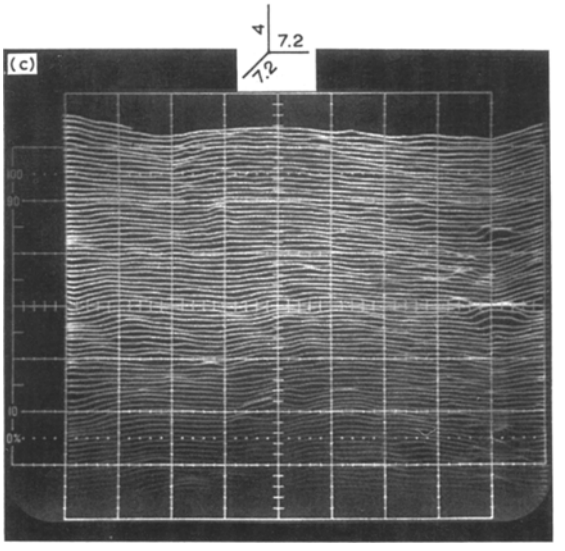

Fig. 11. STM image of iron electrode in solution at $V_{Fe} = -0.75$ V vs NHE; $i_{tun} = 2.0$ nA. (a) after 3 min; (b) after 5 min; (c) after 8 min.

show the image of the electrode obtained after 5 and 8 min, respectively, at the reduction potential. It is observed that the surface became smoother with time, due to the reduction of the oxide film. Similar

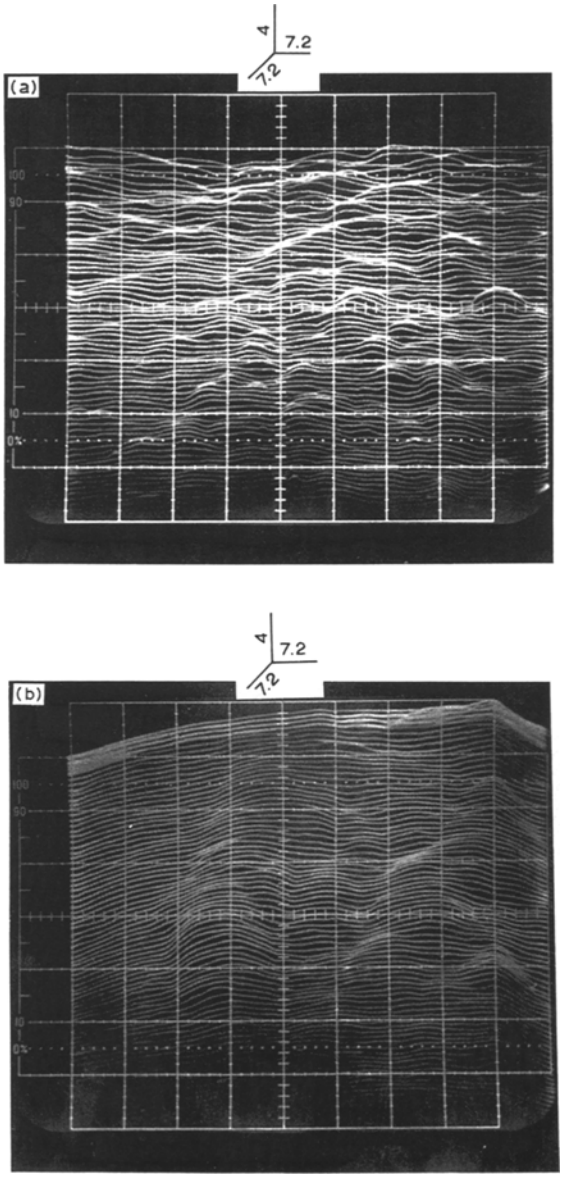

Fig. 12. STM image of iron electrode in solution at $V_{Fe} = -0.355$ V vs NHE; $i_{tun} = 2.0$ nA. (a) immediately after applying potential; (b) after 3 min.

phenomena were observed for aluminium in NaOH solution [9] and stainless steel in aqueous chloride media [14].

Figure 12(a) was taken immediately after applying an anodic potential (−0.355 V vs NHE). Humps of 1 nm height and 3–4 nm width are observed. As for the case of platinum [11] and aluminium [9], a rough surface was produced at high anodic potentials due to the fast rate of oxidation. However, the surface became smoother with time, as shown in Fig. 12(b) (obtained 3 min after applying the anodic potential).

Another interesting result obtained in this work is the observation of a time-dependent modification of the surface during the reduction of an electrochemically grown oxide film (Fig. 13). After applying the reduction potential, the surface looked rough (Fig. 13a). However, after 10 min, the large hemispherical formations were no longer observed, but small humps (Fig. 13b). After these small humps (~1 nm) were formed, the next step was the appearance of a smooth surface in some regions (Fig. 13c, after 13 min). Then, the proportion of the smooth surface kept increasing with time, until the final reduced surface was smooth (Fig. 13d, 15 min).

3.2.4. A kinetic model for electrochemically grown oxides obtained by in situ *STM.* In the case of platinum [11], aluminium [9], and iron [10] it was observed that applying a low anodic potential (~200–400 mV), an oxide film started to be formed as small 'bumps' (~1 nm height and 1–4 nm width) in selected areas of the surface of the electrode (Figs 5, 9 and 12). We do not suppose that only these areas were oxidized, but the electrochemical activity seems to be different in specific places on the surface. In the case of platinum, it is clear that the formation of features took place on steps (Fig. 5). The electrochemical activity at steps is greater than that at terraces. This causes a different mechanism of oxidation of the surface at steps than that at terraces.

In the case of the study of the oxidation–reduction of iron [10], a time-dependent 'reconstruction' of the surface was observed with time during the formation of an electrochemically grown oxide (Fig. 12). At the beginning of the oxidation process, an oxide film (i.e. humps) is formed in selected parts of the surface, i.e. steps. Immediately after an anodic potential is applied, the surface is left with areas having thick oxide film (those where the humps were formed) and areas having thinner oxide film. However, due to the continuous application of the anodic potential, further oxidation is forced. The rate of iron oxidation is faster through the regions where the oxide film is thinner. Thus, if the anodic potential is kept long enough, the final oxide film becomes smooth.

Thus, from these studies of the electrochemical oxidation–reduction of platinum, aluminium and iron by *in situ* STM, some insights at nanometre level of the process have been obtained: (i) oxidation at low anodic potentials seems to start at selective sites on the surface (i.e. steps); (ii) nucleation centres of about 1 nm height and 1–4 nm width are formed during the oxidation of the surfaces of the electrodes at low anodic potentials; (iii) longer times of oxidation produced a smoother surface, due to the growth of the oxide in areas where the oxide is thinner; (iv) in the case of platinum, a mechanism for the reduction of the electrochemically grown oxide is proposed: fast electrochemical reduction, slow crystallographic surface reconstruction, leading to a minimization of the surface energy.

3.3. In situ *corrosion studies of aluminium and Al–Ta alloy in 0.01 M NaCl*

Due to corrosion problems affecting aluminium, new compounds have been searched for, such as aluminium alloys [52] (e.g. Al–Ta alloy [53]).

To compare the corrosion process in aluminium and Al–Ta alloy, it is necessary to monitor changes directly on the surfaces at high resolution. This is

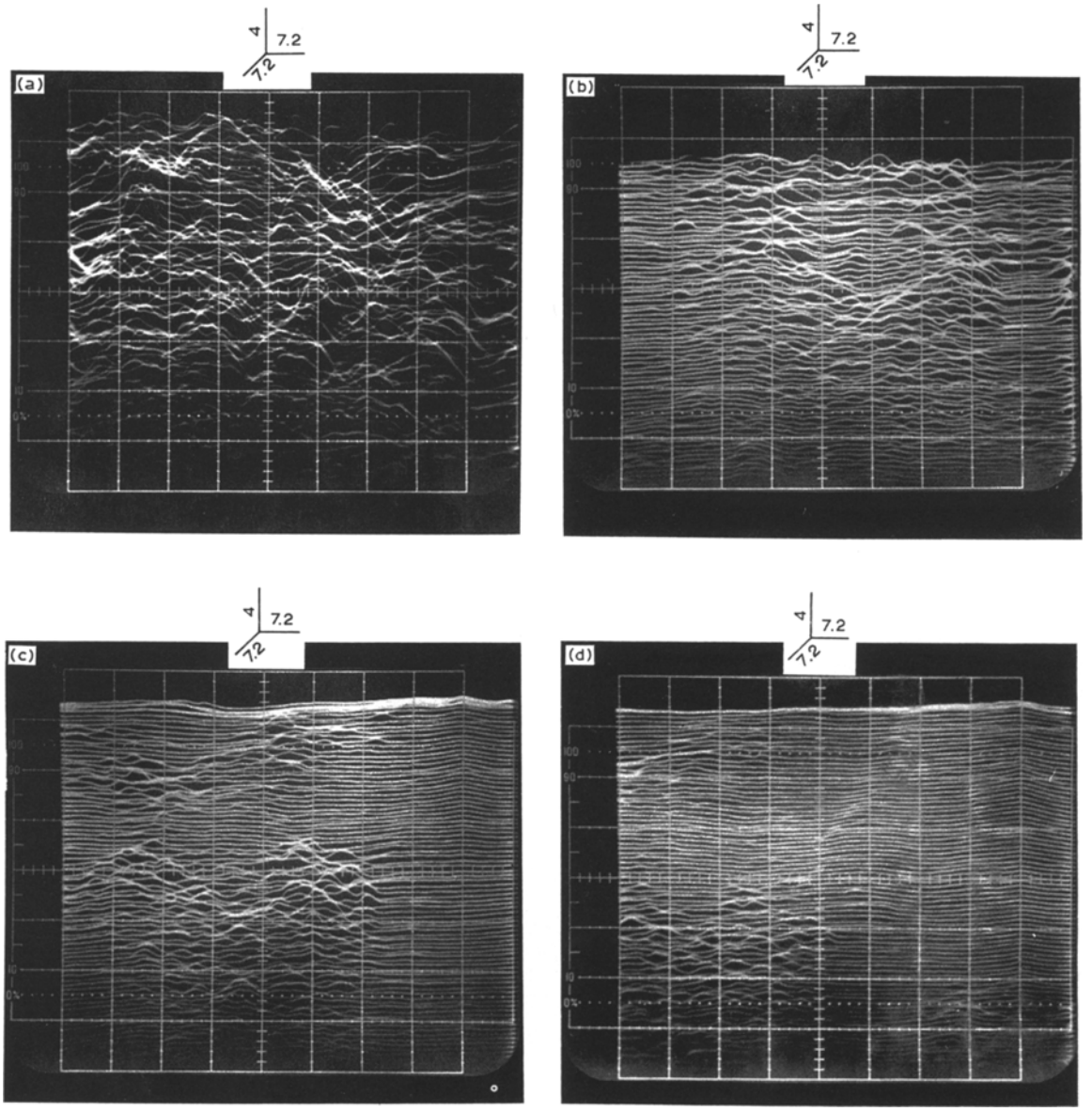

Fig. 13. STM image of iron electrode in solution at $V_{Fe} = -0.75$ V vs NHE; $i_{tun} = 2.0$ nA. (a) after 7 min; (b) after 10 min; (c) after 13 min; (d) after 15 min.

accomplished by *in situ* STM. In this work, the corrosion process on aluminium and Al–Ta alloy electrodes immersed in 0.01 M NaCl is discussed [15].

From the STM experiments, a modification of the surface (i.e. the formation of humps, pits, etc.) as a function of time was observed at the open circuit potential for both the aluminium and the Al–Ta alloy samples immersed in the NaCl solution. The process can be described as a 'roughening' phenomenon when compared with the condition of the initial surface (immediately after immersion).‡

3.3.1. Aluminium STM studies. Figure 14 shows the *in situ* STM image of an aluminium electrode 3 min after it was immersed in the NaCl solution. Well defined steps of 2–4 nm height and terraces of 50–70 nm width and more than 80 nm length are observed.

The progressive modification on the surface topography of the aluminium electrode as a function of time of immersion is depicted in Fig. 15. Figure 15(a) was recorded after 4 h of immersion. The surface structure of the sample was slightly altered. Features of about 4 nm are revealed on the left side of the image. Roughening covers about 50% of the studied area.

After 10 h of immersion, more drastic modifications of the surface were observed (Fig. 15b). Roughening is estimated to cover around 100% of the surface, with features ranging from small bumps of 0.5–1 nm height to V-shape formations (~ 3–4 nm height and ~ 1–2 nm width).

After 17 h of immersion (Fig. 15c), the height of the roughness increased, and V-shape formations and pit-like features spread throughout the surface (1–10 nm height). Severe modification of the surface was observed after 30 h of immersion (Fig. 15d).

‡ A quantification of the 'roughening' process was attempted using two criteria: (i) the percentage of the studied surface that is modified (i.e. formation of humps) after a given time, when compared against a smooth surface; (ii) the size (i.e. height) of such modifications. Within the *z*-resolution, 'roughening' is considered when any feature bigger than 0.5–1 nm appears in the STM image.

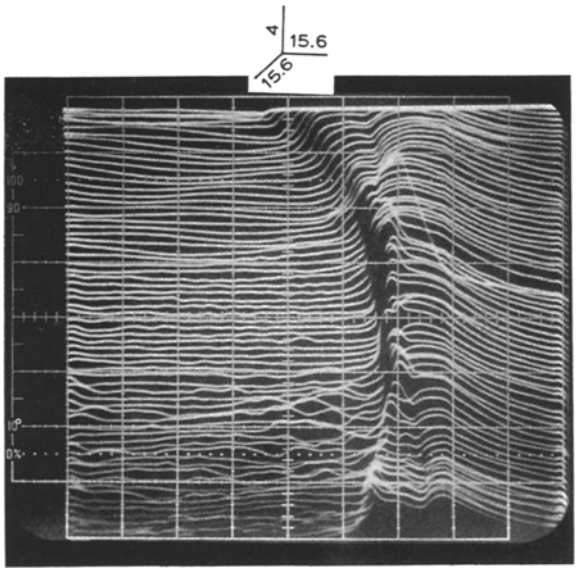

Fig. 14. STM image of aluminium electrode 3 min after immersion in solution. $V_{Al} = -1.20$ V vs NHE; $V_{bias} = -1.05$ V; $i_{tun} = 2.0$ nA.

The percentage of the studied aluminium surface that was modified as a function of time of immersion is shown in Fig. 16.

3.3.2. Al-Ta (8%) STM studies. Figure 17 shows an *in situ* image of the Al–Ta alloy sample 3 min after it was immersed in the NaCl solution. The surface looks smooth with small humps 0.5–1 nm in height and long terraces.

Figure 18a shows the STM image registered *in situ* after 4 h of immersion. Small modifications of the surface (respect to the one just after immersion) are observed in the top right corner ($\sim 20\%$ modification of the surface, 1 nm height).

STM images registered after 10 and 17 h of immersion are shown in Fig. 18(b) and (c), respectively. Modification of the surface was evident after 10 h of immersion (roughness covers around 50% of the studied surface, 1 nm height). However, in any case, the surface of the alloy is 25 to 50% less modified than the aluminium sample, for the same time of immersion (Fig. 15b). After 17 h, about 75% of the surface has been modified (features ranging from 1–2 nm height).

Figure 18(d) shows the image registered after 48 h of immersion. The surface looks very rough (100% of the surface has been modified) with steps of 1–6 nm and terraces of 10–50 nm width. A pit of around 6 nm is visible on the right-hand side of the image. A similar degree of modification was observed for the aluminium sample, but in less time (Fig. 15c, 17 h of immersion).

The percentage of the studied Al–Ta alloy surface that has been modified as a function of time of immersion is shown in Fig. 16.

3.3.3. Corrosion on aluminium electrode against Al–Ta alloy electrode. The STM imaging of both the aluminium and Al–Ta alloy samples in the NaCl solution showed a roughing process with time (Figs 15 and 18). However, the changes observed on the surface of the alloy were not so drastic as for the case of the aluminium sample. It has been determined by XPS that after immersion in 0.1 M NaCl solution, the surface of the alloy is modified due to enrichment by tantalum species [54]. The presence of tantalum species on the surface seems to slow down the process of surface modification, as observed by the STM images. However, the STM image of Al–Ta alloy after 48 h of immersion revealed a pit of 6 nm deep. Thus, eventually the surface enriched by tantalum species ultimately breaks down and pitting starts (i.e. Fig. 18d).

A discussion on the pitting mechanism for both the aluminium and Al–Ta alloy electrodes immersed in the NaCl solution was presented in the original paper [15]. This pitting process causes a local dissolution of the oxide film, which in turn produces a rough surface. This process was indeed observed for both samples (Figs 15 and 18) by *in situ* STM. Initially, the change of the surface is slow: modification on the surface was observed only after 4 h of immersion for the aluminium sample and 10 h for the alloy. The surface was completely modified after 17 h for the aluminium sample, and 24 h for the Al–Ta alloy electrode.

The amount of aluminium dissolved in solution from both aluminium and Al–Ta samples was determined by inductively coupled plasma analysis (ICP). The plot of the dissolution of aluminium as a function of time presented three different regions (Fig. 11 in [15]). From the slope of these three regions, the rate of aluminium dissolution was calculated as a function of time, as shown in Fig. 19.

The highest rate for aluminium dissolution from both samples is found in the first region, Fig. 19, where aluminium species present in the oxide film start to be dissolved immediately after contact with the NaCl solution [55]. However, the rate of aluminium dissolution is about three times faster for the aluminium than for the alloy sample. This result is reasonable considering that the concentration of aluminium species in the oxide on the alloy is less than for the aluminium sample due to the presence of the tantalum species.

For the aluminium sample, the rate of dissolution was slowed down by 10 times after this first region. It was proposed that the precipitation of corrosion products at the outer surface regions of the unprotective oxide film as well as at the porous plugs within the chloride ion penetration channels are responsible for the decrease in the aluminium dissolution [15, 56]. The time required to block the channels was estimated from the ICP analysis, being 30 min.

An increase in the rate of the aluminium dissolution (about five times) is observed after the aluminium sample was immersed for 24 h in the NaCl solution (Fig. 19). This is in agreement with the observations by STM imaging, where a severe modification of the surface occurs after 24 h of immersion (Fig. 15d). This increase in the rate of dissolution may be due to new pitting formation, where unprotected material is exposed to the solution, forcing the dissolution of aluminium.

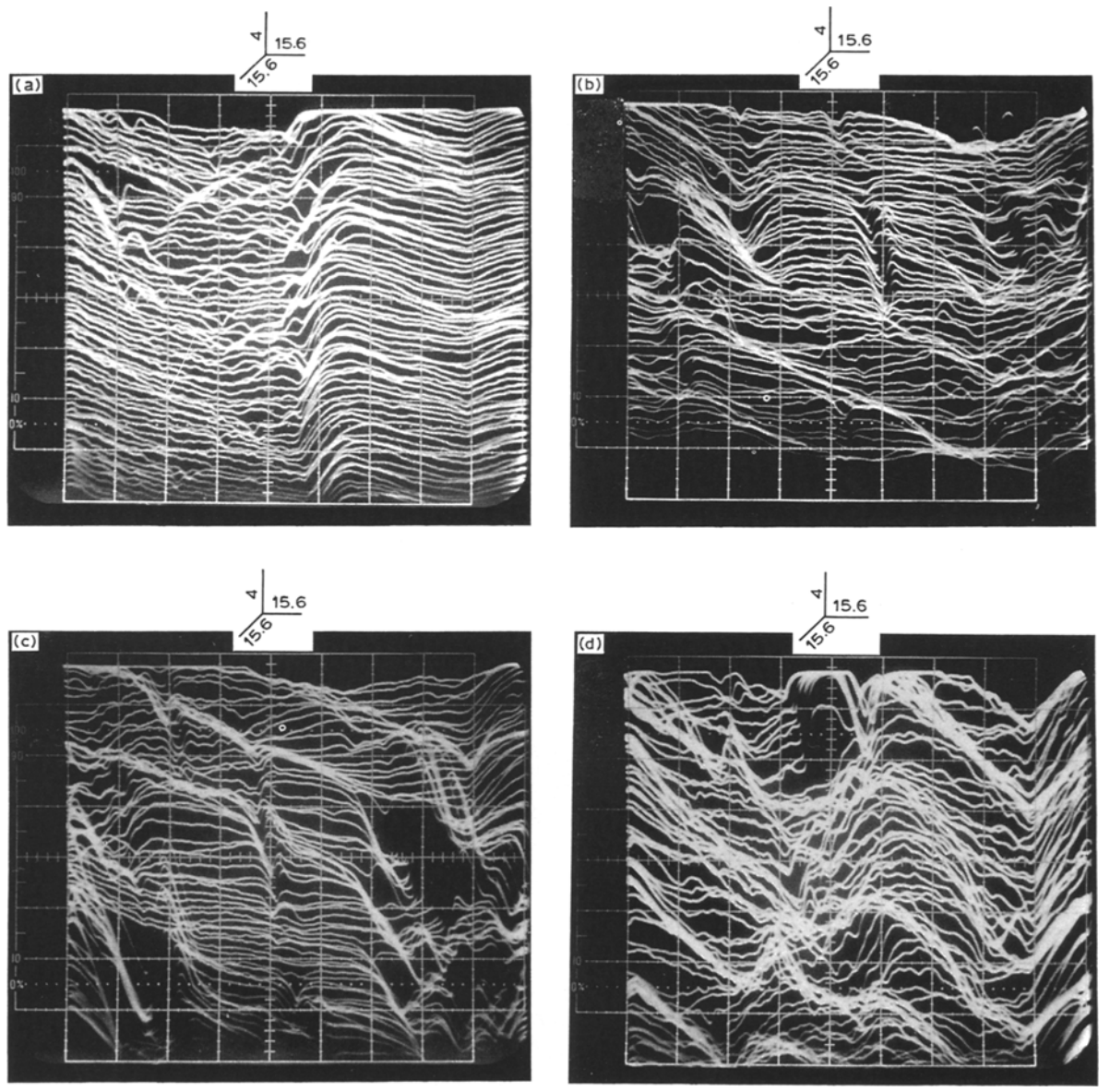

Fig. 15. STM image of aluminium electrode in solution. $V_{Al} = -1.20$ V vs NHE; $V_{bias} = -1.05$ V; $i_{tun} = 2.0$ nA. (a) after 4 h; (b) after 10 h; (c) after 17 h; (d) after 30 h.

For the Al–Ta sample, a second region is also observed, where the rate of aluminium dissolution slowed down by three orders of magnitude. By XPS analysis, it was found that the surface of the alloy was enriched with tantalum species after immersion in 0.1 M NaCl solution [54]. Therefore, presence of tantalum species on the surface slowed down the dissolution process of aluminium, probably by blocking paths used by the Cl^- to reach the oxide/metal interface [57], and by means of the fact that Al–Ta bonds are stronger than Al–Al bonds. However, it seems that the surface enriched by tantalum species ultimately broke down and pitting occurred. This pitting procedure exposed new parts of the alloy to the solution, where dissolution of the aluminium component started all over. This phenomenon was experimentally observed by the ICP analysis (Fig. 19, region 3): after 36 h of immersion, the concentration of aluminium in the solution increased again (by about 25 times). This result is illustrated by the STM imaging of the Al–Ta alloy: after 48 h of immersion a pit of 6 nm deep is revealed. Although the rate of aluminium dissolution increased after 36 h of immersion, the dissolution from the alloy is still about 15 times slower than from the aluminium sample.

Thus, these results (ICP analysis and STM imaging) predict an effective protection against aluminium dissolution ($i_{oc} \sim 3 \times 10^{-7}$ A cm^{-2}) for the Al–Ta alloy sample immersed in 0.01 M NaCl solution up to 36 h. After this time, an increase in the aluminium dissolution rate is found, being about 15 times slower for the Al–Ta alloy than for the aluminium sample.

It is noteworthy that comparison of the ICP and STM results showed that the rate of corrosion is slower in the alloy than in the aluminium sample. This establishes the potential use of the STM for *in situ* imaging of corrosion processes.

3.4. *STM studies of semiconductor surfaces in air and in solution*

Semiconductor materials have been used in the past to split water into hydrogen and oxygen using solar

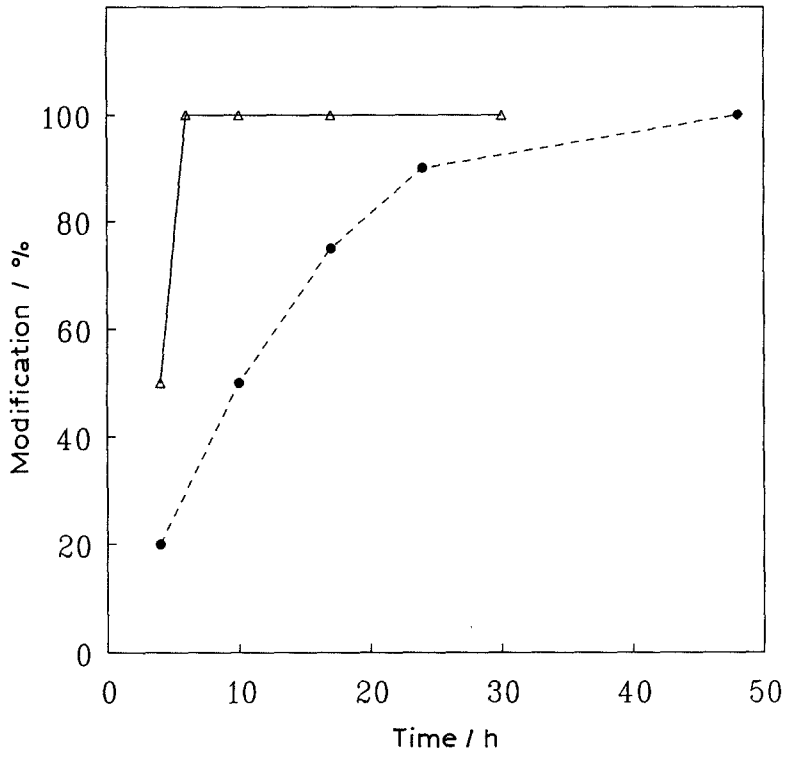

Fig. 16. Roughing process observed by STM as percentage of surface modification as a function of time. (△) Aluminium sample; (●) Al–Ta alloy sample.

energy [58]. However, the efficiency of this process is low, although some improvements are achieved by depositing catalyst particles on the surface of the semiconductor electrodes [59] or by using non-traditional semiconductor materials [60].

A reason for the low efficiency in reactions involving surface adsorbed intermediates is the presence of surface states [61, 62]. Recombination of minority carriers may occur through surface states and prevent the desired reactions between minority carriers and ions in solution. On the other hand, surface states can act directly in electrochemical reactions as intermediate states in electron transfer between the semiconductor bands and ions in solution.

STM has been used in the past to image semiconductor materials (e.g. [63–65]), where silicon is the most extensively studied (e.g. [66 and 67]). Most of the time, high vacuum conditions have been used, allowing studies of surfaces free of oxide. Under these conditions, atomic resolution was obtained [e.g. 67–70]. In addition, correlation between the appearance of the image and surface states and their energies has been attempted [e.g. 68, 69, 71].

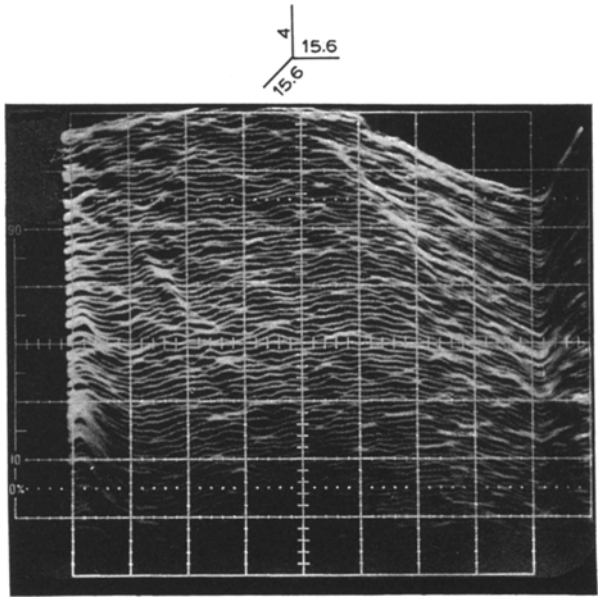

Fig. 17. STM image of Al–Ta electrode 3 min after immersion in solution. $V_{Al\text{-}Ta} = -1.02$ V vs NHE; $V_{bias} = -1.05$ V; $i_{tun} = 2.0$ nA.

STM image of silicon in air is also possible [e.g. 16, 72–75]. However, the STM imaging of silicon in solution is more limited [16, 17, 75–77].

We have used *in situ* STM not only to image the semiconductor (p–Si) surfaces in solution, but also to characterize the semiconductor/solution interface [16, 17]. In this direction, we proposed a new *in situ* method for the detection of surface states and measurement of their energy position. The *in situ* STM studies of p–Si in 0.01 M $NaClO_4$ and in propylene carbonate (PC) containing 0.01 M tetrabutylammonium perchlorate (TBAP) are discussed here. In these studies, the dependance of the STM imaging with the bias potential (potential of the sample respect to the tip) was used as criteria to characterize the properties of the semiconductor surface.

The approach for the STM experiment included: (1) imaging in air, (ii) imaging in solution, and, (iii) imaging in air (after rinsing the electrode with solvent and drying it). Comparison between the conditions required to get STM images allowed to determine modifications introduced by immersing the sample in the solution.

3.4.1. STM imaging of p-Si (1 1 1) in air. Figure 20 shows an STM image of *p*-Si (1 1 1) in air. The surface is made of terraces of dimensions about 20 nm × 40 nm, and 5–10 nm in height. This kind of image was

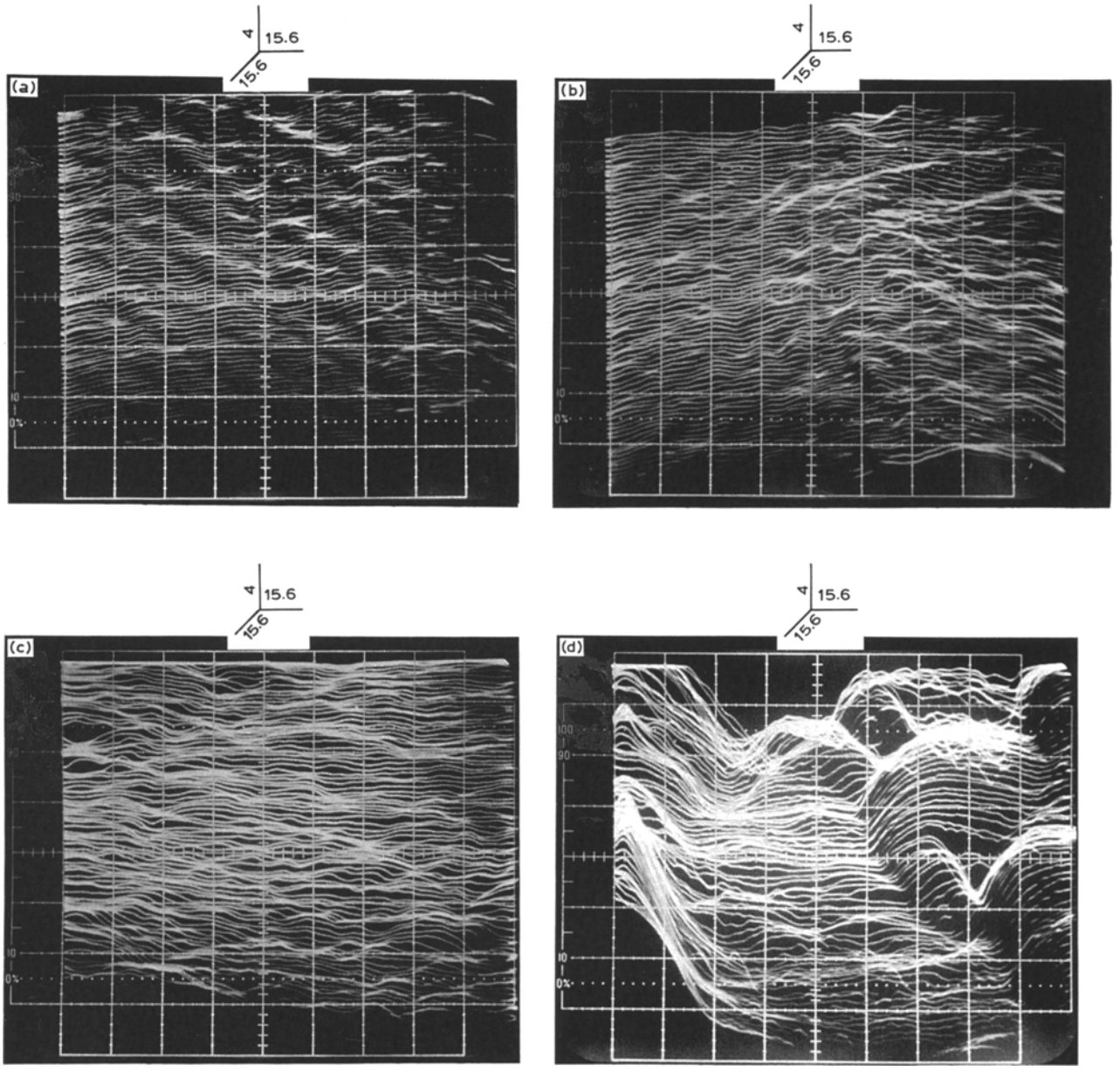

Fig. 18. STM image of aluminium electrode in solution. $V_{Al\text{-}Ta} = -1.05$ V vs NHE; $V_{bias} = -1.05$ V; $i_{tun} = 2.0$ nA. (a) after 4 h; (b) after 10 h; (c) after 17 h; (d) after 48 h.

stable with time. To obtain this image, a positive bias voltage (1.0 V) was applied. Images such as Fig. 20 were obtained as long as the bias voltage was more positive than a threshold value (0.2–0.3 V).

A different situation from that at positive bias voltages was found at negative ones: STM images showed no surface features (for bias up to -1.3 V).

Therefore, for the STM imaging of p-Si in air, images showing surface features are obtained at positive bias voltages (above a threshold value), but not at negative bias voltages (Table 2).

3.4.2. In situ *STM imaging of p-Si (1 1 1) in 0.01 M $NaClO_4$ solution.* Figure 21 shows a STM image of p-Si in 0.01 M $NaClO_4$. The electrochemical potential of the silicon electrode was 0.1 V vs SCE, and the bias voltage was 0.4 V. As observed in air, images showing surface features were recorded at bias voltages more positive than a threshold value (0.2–0.3 V).

A different and surprising result from that in air was found for negative bais voltages in solution. For bias voltages more negative than -0.2 V, STM images showed surface features. Figure 22 was taken at a bias voltage of -0.4 V.

Therefore, for the *in situ* STM imaging of p-Si in 0.01 M $NaClO_4$, images showing surface features are obtained at both positive and negative bias voltages (above a threshold value, Table 2).

Similar behaviour as for the STM imaging in solution was found for the imaging in air *after* the sample was in contact with the solution (sample rinsed and dried). That is, STM images showed surface features at both positive and negative bias voltages (Table 2).

To explain the dependence of the STM imaging of p-Si on the bias voltage, a model based on the induction of surface states in the semiconductor/solution interface is proposed.

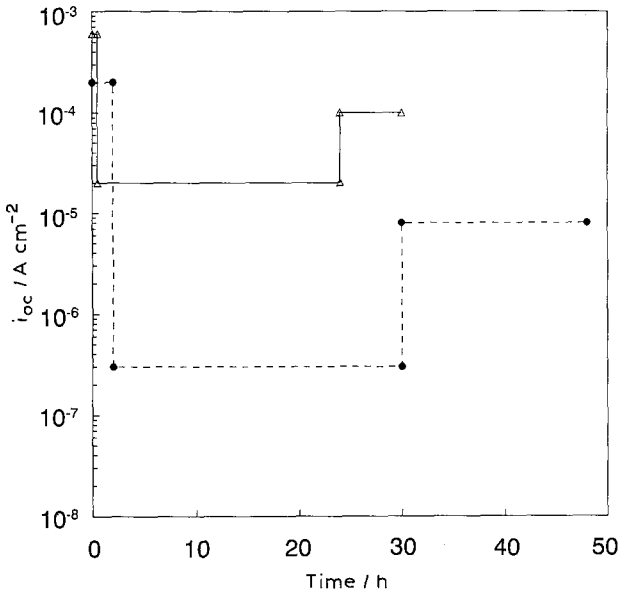

Fig. 19. Rate constant for aluminium dissolution at open circuit potential, I_{oc}, as a function of time. (△) Aluminium sample; (●) Al–Ta alloy sample.

3.4.3. Model for the electron tunnelling in p-Si/oxide/air/tip and p-Si/oxide/solution/tip systems

(a) *p-Si/oxide/air/tip system.* Figure 23 shows an energy/distance diagram for the semiconductor/oxide/air/tip system[§] at zero bias voltage. The slight band bending in p-Si is determined by the difference between the work function of the tungsten tip and the Fermi level of silicon [16]. At zero bias voltage no electrons are transferred.

Table 2. Bias voltage threshold, $V_{threshold}$, needed to observe STM images in the p-Si/oxide/$NaClO_4$/tip system

Bias sign	*Air (Before contact with solution)*	In situ 0.01 M $NaClO_4$	*Air (After contact with solution)*
Positive bias	> 0.2 V	> 0.2 V	> 0.2 V
Negative bias	No image up to −1.3 V	< −0.2 V	< −0.2 V

Applying a bias voltage different from zero either changes the band bending of silicon (no Fermi level pinning situation, NFLP) or shifts the entire silicon energy diagram in respect to the work function of the tungsten tip (Fermi level pinning situation, FLP). If a FLP situation would hold, a barrier for electron transfer from the tip to the sample would always be present. Thus, tunnelling, and therefore imaging, at positive bias voltages would not be possible. Our results show that tunnelling at positive bias voltages indeed took place. In addition, the presence of an oxide film on the silicon surface provides a Si/oxide interface low in surface states. Therefore, a NFLP situation is present in the system.

Figure 24 shows the situation after applying a positive bias voltage such that the bands are moved down. Here, electron tunnelling takes place from the tip to the semiconductor. To reach this situation, positive bias voltages higher than a threshold value has to be applied, in agreement with our results (Table 2).

At negative bias voltages, two situations can be depicted (Figs 25 and 26). At low negative bias voltages (Fig. 25, situation shown as (a)), electrons from

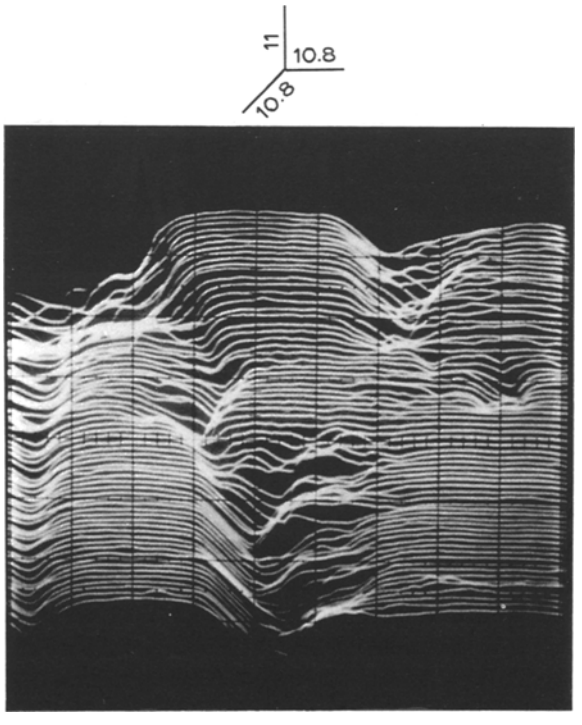

Fig. 20. STM image of p-Si in air; V_{bias} = 1.0 V; i_{tun} = 1.0 nA.

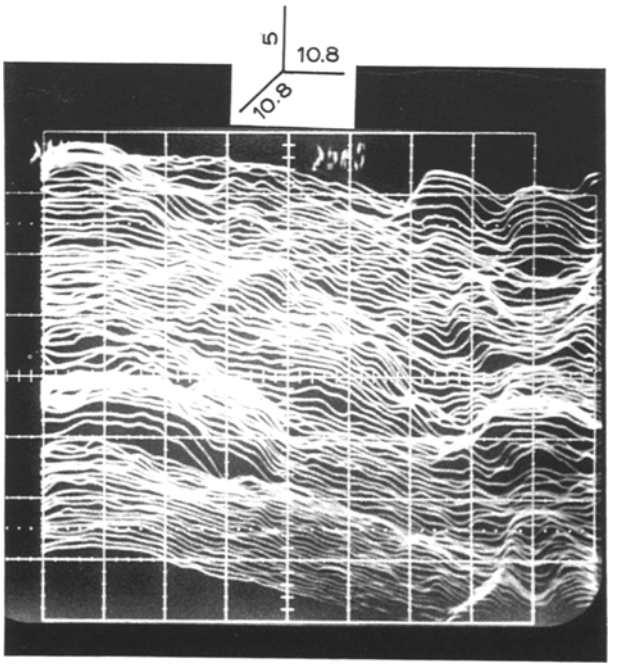

Fig. 21. STM image of p-Si in solution. E_{Si} = 0.1 V vs SCE; V_{bias} = 1.0 V; i_{tun} = 1.0 nA.

§ By XPS studies [17] it is known that the initial silicon surface contains a native oxide.

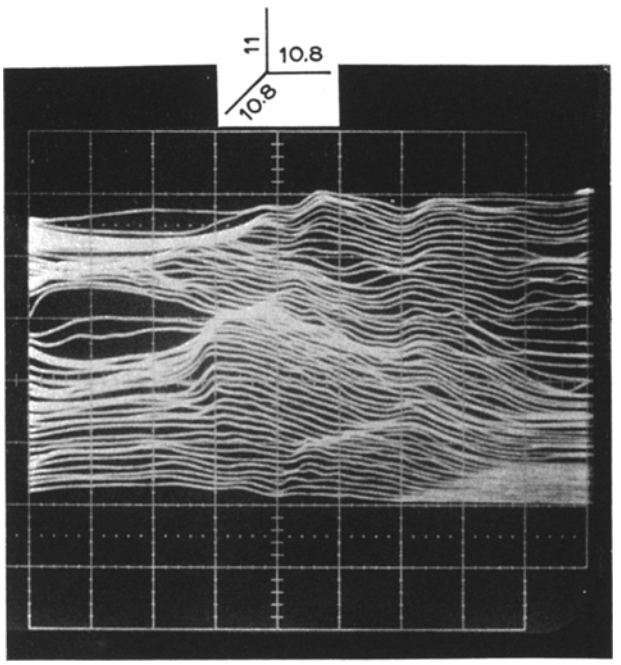

Fig. 22. STM image of p-Si in solution. $E_{Si} = -0.4$ V vs SCE; $V_{bias} = -0.4$ V; $i_{tun} = 1.0$ nA.

the valence band of the semiconductor do not find empty states on the tip. Therefore, tunnelling does not take place. By applying more negative bias voltages, the situation shown in Fig. 25, situation (b), is reached. In this case, electron tunnelling would take place if the distance for tunnelling is not bigger than 2–3 nm. However, due to the presence of the space charge region and the oxide film, this distance is too big to allow electron tunnelling.

By applying much higher negative bias voltages, the situation shown in Fig. 26 may be reached, where electrons can be thermally excited from the valence band to the bottom of the conduction band. Once in the conduction band, electron tunnelling would take place because the distance to tunnel has been reduced to the oxide film (less than 2 nm [17]) and the gap between the surface of the sample and tip (as low as a few nanometres or less). However, this situation was never reached within the values of bias voltages that we used (below -1.3 V).

This model explains why it was not possible to obtain STM images showing surface features in air at

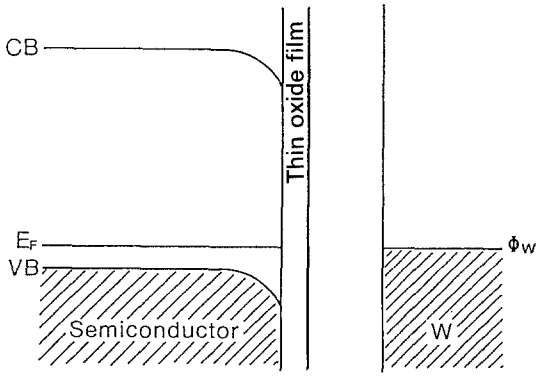

Fig. 23. Energy distance diagram for p-Si/oxide/air/tip system at $V_{bias} = 0$ V.

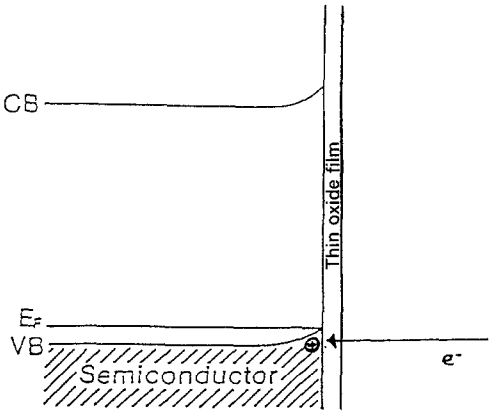

Fig. 24. Energy distance diagram for p-Si/oxide/air/tip system at positive bias voltages.

negative bias voltages.

(b) *p-Si/oxide/solution/tip system.* At positive bias voltages, the situation is not much different from the condition in air, because of the presence of the silicon oxide: a Schottky model holds, so the potential changes are mainly occurring in the space charge region of the semiconductor.

However, the situation at negative bias voltages is different from the case in air, because imaging of the surface was possible in solution (after a threshold value) but not in air (previous to immersion), Table 2.

By applying negative bias, bands are raised. If states are available at the silicon oxide surface, electrons from the valence band of the semiconductor can reach those states, and then electrons can tunnel from those states to the tip (Fig. 27), so images showing surface features can be recorded. We propose that these states on the silicon oxide are surface states induced by the immersion of the semiconductor surface in solution. Respect to the nature of these states, they may be due to adsorption of species present in solution or modification of the nature of the oxide film (i.e. by electrochemical formation of SiO_x and/or Si–OH [78]). In any case, these surface states are not removed by rinsing and drying the electrode surface, because images showing surface features were obtained at

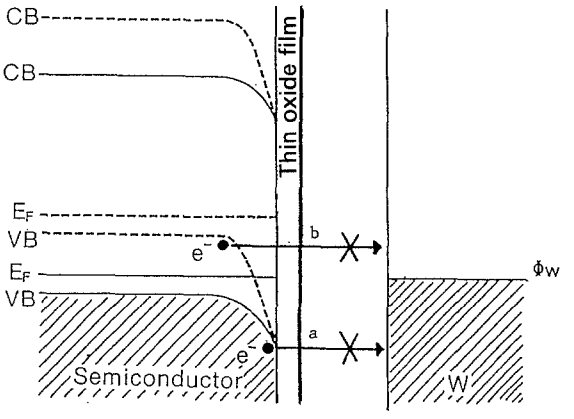

Fig. 25. Energy distance diagram for p-Si/oxide/air/tip system at negative bias voltages.

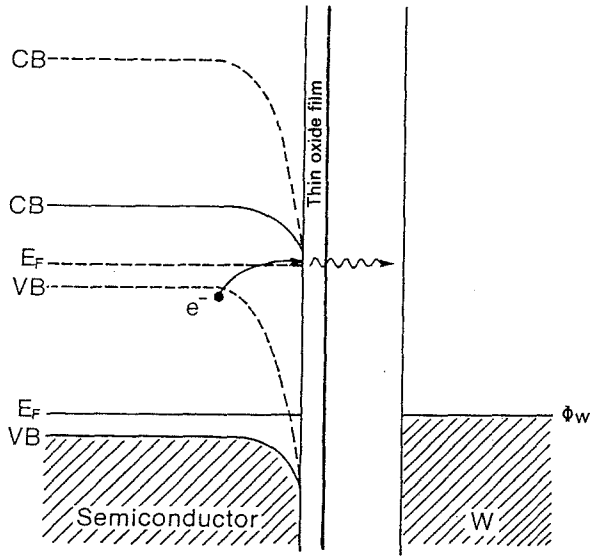

Fig. 26. Energy distance diagram for p-Si/oxide/air/tip system at high negative bias voltage.

negative bias for the sample in air *after* contact with solution.

Using this model, a value for the energy position of this band of surface states was estimated [16]. It was obtained that these states were located at about 0.25–0.35 eV above the energy position of the valence band in the Si/oxide interface. This value is in good agreement with the one determined by an independent technique, sub-band gap photocurrent spectroscopy [79]. The value obtained there is 0.3 eV.

3.4.4. In situ STM imaging of p-Si(1 1 1) in 0.01 M TBAP (PC) solution. Using the same principle as for the *p*-Si/$NaClO_4$ system, we used STM to study the *p*-Si/TBAP (PC) interface [17]. In this system, a band of surface states was determined to be induced in solution. Its energy position was calculated to be 0.55–0.65 eV above the energy position of the valence band at the semiconductor/oxide interface.

Thus, we have proved that STM is a powerful technique for the detection of surface states which are induced in the semiconductor/solution interface. In addition, the energy position of these states can be estimated.

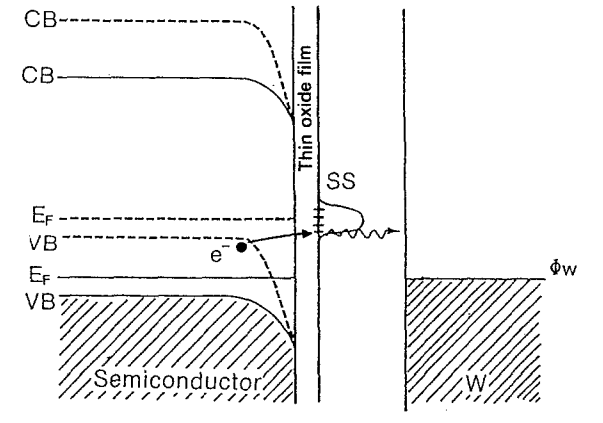

Fig. 27. Energy distance diagram for p-Si/oxide/solution/tip system at negative bias voltages.

4. Conclusions

STM has been proved as a powerful technique for the *in situ* studies of electrode surfaces at high resolution (atomic to μm). Insights on the mechanisms of electrochemical reactions and characterization of electrode-solution interfaces are obtained by *in situ* STM studies.

Among the contributions from our group to *in situ* STM studies in electrochemistry are the following:

(i) The atomic resolution of electrodeposited lead in air and in electrolytic solution was achieved for the first time.

(ii) The oxidation of metallic surfaces at low anodic potentials starts with the formation of small features (1–4 nm) in selected places of the electrode (i.e. steps). A time-dependent process is observed by forcing further electrochemical oxidation of the surface, which becomes smooth in a 10 nm to 1 μm scale.

(iii) A mechanism was proposed for the reduction of electrochemically grown oxides: fast electrochemical reduction, slow crystallographic surface reconstruction.

(iv) Direct comparison of the corrosion process between aluminium and Al–Ta alloy was obtained. An effective protection against aluminium dissolution from the alloy was shown for the first 36 h of immersion in a NaCl solution.

(v) A new method for the detection of surface states and their energy position was proposed by the *in situ* characterization of the semiconductor-solution interfaces. In the case of *p*-Si/$NaClO_4$ interface, a band of surface states was permanently induced *after* the electrode was in contact with the solution. The energy of this band was 0.25–0.35 eV above the energy position of the valence band at the Si/oxide interface. In the *p*-Si/TBAP (PC) interface, a band of surface states was permanently induced *after* the electrode was oxidized. The energy of this band was 0.55–0.65 eV.

Acknowledgement

The authors wish to thank Dr M. Szklarczyk and O. Velev who carried out part of the experimental work discussed here. The Welch Foundation, ONR and SERI are also acknowledged for their financial support.

References

[1] Oberlech, 1985, *IBM J. Res. Develop.* **30**(4/5) (1986).
[2] A. J. Arvia, *in* 'Spectroscopy and Diffraction Techniques in Interfacial Electrochemistry', (edited by C. Gutierres and C. Melendres), Kluwer Academic Publishers, Boston (1990).
[3] R. Sonnenfeld and P. K. Hansma, *Science* **232** (1986) 211.
[4] R. Christoph, H. Siegenthaler, H. Rohrer and H. Wiese, *Electrochim. Acta.* **14** (1989) 1011.
[5] M. Szklarczyk and J. O'M. Bockris, *J. Electrochem. Soc.* **137** (1990) 452.
[6] R. S. Robinson, *J. Vac. Sci. Technol.* **A8** (1990) 511.
[7] C. M. Vitus, S.-C. Chang, B. C. Schardt and M. J. Weaver, *J. Phys. Chem.* **95** (1991) 7559.
[8] K. Uosaki and H. Kita, *J. Vac. Sci. Technol.* **A8** (1990) 520.
[9] R. C. Bhardwaj, A. González-Martín and J. O'M. Bockris, *J. Electroanal. Chem.* **307** (1991) 195.

[10] R. C. Bhardwaj, A. González-Martín and J. O'M. Bockris, *J. Electrochem. Soc.* **138** (1991) 1901.
[11] M. Szklarczyk and J. O'M. Bockris, *Surf. Sci.* **241** (1991) 54.
[12] K. Sashikata, N. Furuya and K. Itaya, *J. Vac. Sci. Technol.* **B9** (1991) 457.
[13] J.-S. Chen, T. M. Devine, D. F. Ogletree and M. Salmeron, *Surf. Sci.* **258** (1991) 346.
[14] F.-R. F. Fan and A. J. Bard, *J. Electrochem. Soc.* **136** (1989) 166.
[15] R. C. Bhardwaj, A. González-Martín and J. O'M. Bockris, *ibid.* **139** (1992) 1050.
[16] M. Szklarczyk, A. González-Martín, O. Veleva and J. O'M Bockris, *Surf. Sci.* **239** (1990) 305.
[17] M. Szklarczyk, A. González-Martín and J. O'M. Bockris, *ibid.* **257** (1991) 307.
[18] P. Carlsson, B. Holmstrom, H. Kita and K. Uosaki, *ibid.* **237** (1990) 280.
[19] K. Itaya, R. Sugawara, Y. Morita and H. Tokumoto, *Appl. Phys., Lett.* **60** (1992) 2534.
[20] M. Szklarczyk, O. Velev and J. O'M. Bockris, *J. Electrochem. Soc.* **136** (1989) 2433.
[21] J. Wintterlin, J. Wiechers, H. Brune, T. Critsch, H. Hofer and R. J. Behm, *Phys. Rev. Lett.* **62** (1989) 59.
[22] V. M. Hallmark, S. Chiang, J. F. Rabot, J. D. Swalen and R. J. Wilson, *Phys. Rev. Lett.* **59** (1987) 2879.
[23] B. C. Schardt, *Science* **243** (1989) 1050.
[24] T. Gritsch, D. Coulman, R. J. Behm and G. Ertl, *Appl. Phys. A* **49** (1989) 403.
[25] W. L. Bragg and J. A. Darbyshire, *Trans. Faraday Soc.* **28** (1932) 522.
[26] 'CRC Handbook of Chemistry and Physics', (edited by R. C. Weast and M. J. Astle) 60th edn, CRC Press, Ohio (1980).
[27] Quantum mechanical value for diameter of free atom. Reported in 'Table of Periodic Properties of the Elements' (Sargent–Welch Scientific Company, Skokie, IL, 1979).
[28] W. J. Moore, Jr. and L. Pauling, *J. Am. Chem. Soc.* **63** (1941) 1392.
[29] S. M. Kochergin, *Zh. Tekn. Fiz.* **23** (1953) 955.
[30] K. M. Gorbunova, O. S. Popova, A. A. Sytyagina and Y. Polukav, Reports at the 1st Conference on Crystal Growth, Moscow, 5–10 March (1956) p. 58.
[31] S.-L. Yau, C. M. Vitus and B. C. Schardt, *J. Am. Chem. Soc.* **112** (1990) 3677.
[32] C. M. Vitus, S.-C. Chang, B. C. Schardt and M. J. Weaver, *J. Phys. Chem.* **95** (1991) 7559.
[33] S.-L. Yau, X. Gao, S.-C. Chang, B. C. Schardt and M. J. Weaver, *J. Am. Chem. Soc.* **113** (1991) 6049.
[34] F. Besenbacher, F. Jensen, E. Laegsgaard, K. Mortensesn and I. Stensgaard, *J. Vac. Sci. Technol.* **B9** (1991) 874.
[35] D. F. Ogletree, R. Q. Hwang, D. M. Zeglisnki, A. Lopez Vazquez-de-Parga, G. A. Somorgai and M. Salmeron, *ibid.* **B9** (1991) 886.
[36] S. Manne, J. Massie, V. B. Elings, P. K. Hasma and A. A. Gewirth, *ibid.* **B9** (1991) 950.
[37] O. M. Magnussen, J. Hotlos, G. Beitel, D. M. Kolb and R. J. Behm, *ibid.* **B9** (1991) 969.
[38] J. W. M. Frenken, R. J. Hamers and J. E. Demuth, *ibid.* **A8** (1990) 293.
[39] G. Binning and H. Rohrer, *Helv. Phy. Acta.* **55** (1982) 726.
[40] L. Vazquez, J. M. Gomez Rodriguez, J. Gomez Herrero, A. M. Baro, N. Garcia, J. C. Canullo and A. J. Arvia, *Surf. Sci.* **181** (1987) 98.
[41] K. Itaya, S. Sugawara and K. Higaki, *J. Phys. Chem.* **92** (1988) 6714.
[42] K. Itaya, S. Sugawara, K. Sashikata and N. Furuya, *J. Vac. Sci. Technol.* **A8** (1990) 515.
[43] I. Otsuka and T. Iwasake, *J. Microsc.* **152** (1988) 989.
[44] V. Jovancicevic, R. C. Kainthla, Z. Tang, B. Yang and J. O'M. Bockris, *Langmuir* **3** (1987) 388.
[45] W. C. Moshier, G. D. Cavis, J. S. Ahearn and H. F. Hough, *J. Electrochem. Soc.* **136** (1989) 356.
[46] P. M. Natishan, E. McCafferty and G. K. Gubler, *Mater. Sci. & Eng.* **A116** (1989) 41.
[47] A. Miyamaka and H. Ogawa, *Corros. Sci.* **46** (1990) 99.
[48] F.-R. F. Fan and A. J. Bard, *Anal. Chem.* **60** (1988) 751.
[49] M. Szklarczyk, Lj. Minevski and J. O'M. Bockris, *J. Electroanal. Chem.* **289** (1990) 279.
[50] S. Real, M. Urquidi-MacDonald and D. D. MacDonald, *J. Electrochem. Soc.* **135** (1988) 1633.
[51] D. D. MacDonald, S. Real and M. Urquidi-MacDonald, *ibid.* **135** (1988) 2397.
[52] W. C. Moshier, G. D. Davis and G. O. Cole, *ibid.* **133** (1986) 1063.
[53] G. D. Davis, W. C. Moshier, T. L. Fritz and G. O. Cole, Martin Marieta Laboratories, Annual Report, Jan. 1989.
[54] R. C. Bhardwaj, N. Smart and J. O'M. Bockris, *J. Electrochem. Soc.* in press.
[55] R. T. Foley, *Corrosion (Houston)* **42** (1986) 277.
[56] O. J. Murphy, T. E. Pou and J. O'M. Bockris, *J. Electrochem. Soc.* **131** (1984) 2785.
[57] W. C. Moshier, G. D. Davis, J. S. Ahearn and H. F. Hough, *ibid.* **134** (1987) 2677.
[58] A. Heller, *Science* **223** (1984) 1141.
[59] R. C. Kaintla, B. Zelenay and J. O'M. Bockris, *J. Electrochem. Soc.* **134** (1987) 841.
[60] D. Montgomery, S. S. Kocha, J. A. Turner and A. J. Nozik, Proceedings of the DOE/SERI Hydrogen Program, Washington (1991).
[61] J. F. McCann and D. Haneman, *J. Electrochem. Soc.* **104** (1982) 1134.
[62] H. Gerischer, *in* 'Electronic and Molecular Structure of Electrode–Electrolyte Interface', (edited by W. N. Hansen, D. M. Kolb and D. W. Lynch), Elsevier, New York (1983).
[63] A. Humbert, F. Salvan and C. Mouttet, *Surf. Sci.* **181** (1987) 307.
[64] J. A. Stroscio and F. M. Feenstra, *J. Vac. Sci. Technol.* **B6** (1988) 1472.
[65] K. Itaya and E. Tomita, *Chem. Lett.* (1989) 285.
[66] J. A. Stroscio, R. M. Feenstra, D. M. Newns and A. P. Tein, *J. Vac. Sci. Technol.* **A6** (1988) 499.
[67] M. E. Welland and R. H. Koch, *Appl. Phys. Lett.* **46** (1986) 724.
[68] R. J. Hamers, R. M. Tromp and J. E. Demuth, *Surf. Sci.* **181** (1987) 346.
[69] R. M. Tromp, *J. Phys., Condens. Matter.* **1** (1989) 10211.
[70] Ph. Avouris and I.-W. Lyo, *Surf. Sci.* **242** (1991) 1.
[71] R. Wolkow and Ph. Avouris, *Phys. Rev. Lett.* **60** (1988) 1049.
[72] K. H. Besocke, M. Tekde and J. Frohn, *J. Vac. Sci. Technol.* **A6** (1988) 408.
[73] I. Tanaka, F. Osaka, T. Kato, T. Katayama, S. Muramatsu and T. Shimada, *Appl. Phys. Lett.* **54** (1989) 427.
[74] Y. Nakagawa, A. Ishitani, T. Takahagi, H. Kuroda, H. Tokumoto, M. Ono and K. Kajimura, *J. Vac. Sci. Technol.* **A8** (1990) 262.
[75] E. Tomita, N. Matsuda and K. Itaya, *ibid.* **A8** (1990) 534.
[76] J. P. Carrejo, T. Thundat, L. A. Nagahara, S. M. Lindsay and A. Majumdar, *ibid.* **B9** (1991) 955.
[77] K. Itaya, R. Sugawara, Y. Morita and H. Tokumoto, *Appl. Phys. Lett.* **60** (1992) 2534.
[78] M. Szklarczyk, J. O'M. Bockris, V. Brusic and G. Sparrow, *Int. J. Hydrogen Energy* **9** (1984) 707.
[79] A. González-Martín, Dissertation, Texas A & M University (1992).